Theor Chem Acc (2012) 131:1250
DOI 10.1007/s00214-012-1250-7

REGULAR ARTICLE

Calculation of solvation free energies of Li^+ and O_2^- ions and neutral lithium–oxygen compounds in acetonitrile using mixed cluster/continuum models

Vyacheslav S. Bryantsev

Received: 9 June 2012 / Accepted: 19 June 2012 / Published online: 3 July 2012

Abstract Solvation effects play a major role in determining the cycling characteristics of the non-aqueous rechargeable Li-air battery. We use a mixed cluster/continuum solvent model with varying number of explicit solvent molecules ($n = 4$–10) to calculate the solvation free energies (ΔG^*_{solv}) of Li^+ and O_2^- ions and neutral LiO_2, Li_2O_2, LiO, and Li_2O species in acetonitrile solvent. Calculations for complexes with the full first solvation shell around Li^+ ($n = 4$) and O_2^- ($n = 8$) show excellent agreement with the solvation free energies obtained using the cluster pair approximation (the error is below 2.0 kcal/mol). The use of the pure continuum model fitted to reproduce the experimental values of $\Delta G^*_{solv}(Li^+)$ and $\Delta G^*_{solv}(O_2^-)$ gives the solvation free energies of various lithium–oxygen species (Li_xO_y; x, $y = 1$, 2) that are in excellent agreement with the results obtained using mixed cluster/continuum models ($n \geq 8$). This provides a theoretical framework for including solvent effects in the theoretical models of oxygen reduction and evolution reactions in the aprotic Li-air battery.

Keywords Solvation free energy · Continuum and mixed cluster/continuum solvent models · Lithium ion · Superoxide ion · Lithium–oxygen compounds · Acetonitrile solvent

V. S. Bryantsev (✉)
Liox Power, Inc., 129 N. Hill Ave., Suite 103, Pasadena, CA 91106, USA
e-mail: slava@wag.caltech.edu; slava@liox.com

1 Introduction

Solvent plays a major role in determining the nature of discharge products and the extent of rechargeability of the non-aqueous lithium-air (oxygen) battery [1]. The foremost challenge is to find a stable electrolyte composition that allows the reversible formation and decomposition of Li_2O_2 during cell cycling [2–4]. Solvent decomposition during oxygen reduction has been recognized as a major problem when employing carbonate-based electrolytes [5–12]. Several classes of electrolyte solvents with improved stability against oxygen reduction products have been reported recently [8, 13–18]. A better understanding of how solvent properties affect Li_2O_2 rechargeability in stable electrolyte compositions is critical for achieving long-term cycling of the Li-air battery [4].

Solvation phenomena play an important role in the cycling characteristics of the O_2 electrode. For example, solvation may affect (1) the thermodynamic stability of reaction intermediates (e.g., LiO_2), (2) the potential-dependent lithium–oxygen surface phase diagram, and iii) the morphology and distribution of discharge products. Additionally, enhanced solubility of discharge products may enable more efficient recharging, since bulk Li_2O_2 and Li_2O are electronic insulators. Despite the critical role played by the solvent in determining the positive electrode chemistry, theoretical analysis of elementary oxygen reduction (ORR) and oxygen evolution (OER) reactions in the aprotic Li-air battery reported so far have omitted discussion of solvent effects [19–23]. The lack of consideration of solvent effects could be a reflection of difficulties to incorporate explicit electrolyte models in periodic density functional theory (DFT) calculations (but see Refs. [24–26]) and also due to insufficient parameterization of continuum solvation models for ionic compounds

containing Li and O atoms in non-aqueous electrolytes. A correct account of complexation of Li^+ with O_2^- and O_2^{2-} also requires accurate calculations of the solvation free energies for ions, which has proved to be difficult to compute reliably, since the results are sensitive to the choice of computational and cluster models [27–31]. Recent developments in the computational protocols for systems involving strongly solvated ions enable systematic improvements of the calculated solvation free energies with increasing the level of theory and cluster size [27–31].

Herein, we employ first-principles calculations for predicting the solvation free energies of Li^+ and O_2^- ions and neutral LiO_2, Li_2O_2, LiO, and Li_2O species in CH_3CN. Acetonitrile is chosen as a solvent in this study because it is sufficiently stable towards reduced O_2 species [32] and provides important experimental data to benchmark the theoretical predictions [33]. Solvation of charged and ionic solutes is modeled by explicit inclusion of solvent molecules in the vicinity of the ion and implicit treatment of the rest of the solvent with a dielectric continuum model [28]. This mixed cluster/continuum framework avoids the ambiguities of assigning atomic radii for highly ionic Li and O, because the results are not sensitive to the choice of these parameters if a solute is completely surrounded by solvent molecules. Excellent agreement with the experimental solvation free energies of Li^+ and O_2^- obtained from studies of ion-acetonitrile clusters [33] provides strong support for the computational model, thereby lending credence to the calculated solvation free energies of various Li_xO_y (x, $y = 1$, 2) species. Furthermore, we find that pure continuum solvent models utilizing solute radii of Li and O fitted to reproduce the solvation free energies of Li^+ and O_2^- are able to describe accurately the solvation thermodynamics of LiO_2, Li_2O_2, LiO, and Li_2O species, involving oxygen in three different oxidation states. This provides a justification for the use of continuum solvation models, if properly parameterized, to estimate the solvation effects for the elementary reaction steps involved in ORR and OER in aprotic solvents.

2 Theoretical methods

2.1 Calculation of solvation free energies using mixed cluster/continuum models

Solvation free energies of charged and neutral polar solutes ($A^{m\pm}$) were calculated using the thermodynamic cycle (cluster cycle) shown in Scheme 1. Previous studies [28] showed that due to a favorable compensation of errors in the applied cluster/continuum model, the cluster cycle with $(solvent)_n$ cluster as a reagent provides more accurate solvation free energies compared to the monomer cycle

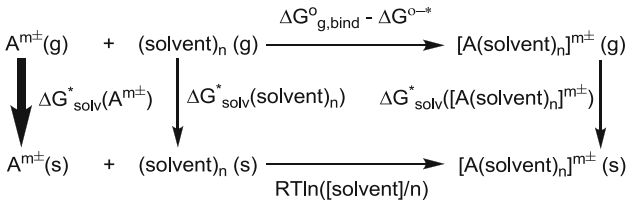

Scheme 1 Thermodynamic cycle for the calculation of $\Delta G^*_{solv}(A^{m\pm})$

with n distinct solvent molecules as reagents. In Scheme 1, $\Delta G^o_{g,bind}$ is the gas-phase complexation free energy ($\Delta G^o_{g,bind}$), $\Delta G^*_{solv}(X)$ is the free energy of solvation for $X = A^{m\pm}$, $(solvent)_n$, and $[A(solvent)_n]^{m\pm}$, $\Delta G^{o\to *}_{solv} = RT\ln(24.46) = 1.89$ kcal/mol ($T = 298.15$ K) is the free energy change of 1 mol of gas from 1 atm (24.46 L mol^{-1}) to 1 M (1 mol L^{-1}), and RT ln([solvent]/n) is the free energy change of 1 mol of $(solvent)_n$ gas from [solvent]/n M liquid state to 1 M. $\Delta G^{o\to *}_{solv}$ and RT ln([solvent]/n) are the standard state correction terms that must be applied to bring each reactant and product in the thermodynamic cycle to the same standard state (1 M) [28]. From Scheme 1, $\Delta G^*_{solv}(A^{m\pm})$ is given by

$$\begin{aligned}\Delta G^*_{solv}(A^{m\pm}) = {} & \Delta G^o_{g,bind} + \Delta G^*_{solv}\left([A(solvent)_n]^{m\pm}\right) \\ & - \Delta G^*_{solv}((solvent)_n) - \Delta G^{o\to *} \\ & - RT\ln([solvent]/n). \end{aligned} \quad (1)$$

2.2 Gas-phase calculations

Electronic structure calculations were carried out using the Jaguar 7.7 [34] and the NWChem 5.1.1 [35, 36] programs. We examined the ability of four density functionals including one hybrid GGA (B3LYP) [37, 38], one local meta-GGA (M06-L) [39], and two hybrid meta-GGAs (M06 and M06-2X) [40] to reproduce the experimental enthalpies and free energies of complexation in the gas phase (see Sect. 4.1). For these functionals two basis sets were considered: 6-311++G^{**} and aug-cc-pVTZ [41, 42]. The geometries of all clusters with four acetonitrile molecules ($n = 4$) were optimized with the 6-311++G^{**} basis set. Clusters with $n = 6$, 8, and 10 were optimized using the 6-31G^{**} basis set, followed by single-point energy calculations with the 6-311++G^{**} or aug-cc-pVTZ basis set. Control calculations for $O_2^-(CH_3CN)_8$ and $Li_2O_2(CH_3CN)_8$ shows that this procedure leads to the calculated solvation free energies (Eq. 1) that differ by 0.5–1.0 kcal/mol when compared to results obtained after full optimization at the B3LYP/6-311++G^{**} level. Vibrational frequencies were computed analytically at the B3LYP/6-31G^{**} level. The standard Gibbs free energy of each species in the gas phase was calculated using the rigid rotor—harmonic oscillator approximation without scaling.

2.3 Implicit solvation calculations

Continuum solvation calculations were carried out using the Poisson-Boltzmann (PB) model as implemented in Jaguar [34]. The electronic energies in the solvent reaction filed were obtained at the B3LYP/6-311++G^{**} and M06-L/6-311++G^{**} levels. Solvation calculations were carried out in acetonitrile (MeCN) using a dielectric constant of 35.97 and the probe radius of 2.180 Å. The choice of atomic radii that determine the van der Waals envelope of the solute is critical for accurate estimation of solvation effects with implicit models. Most continuum models of the solvent provide default atomic radii optimized for neutral organic molecules in water. Using the default atomic radii in Jaguar resulted in considerable discrepancies between the calculated and experimental solvation free energies for the neutral solutes (see Sect. 4.2). These differences were minimized by uniform scaling of the default solvation radii by 1.40. Test calculations were also performed using the Jaguar version of the SM8 solvation model [43, 44] used together with the M06 density functional and the 6-31G^{*} basis set.

Zuo et al. [45] have recently fitted metal ion atomic radii used with the IEFPCM solvent model [46, 47] to match the experimental absolute free energies of hydration. This provided improved agreement with the stability constant measured for a series of pyridine-based ligands in water compared to the results obtained using the default UAHF ion radii [48]. Following a similar strategy, we obtained a new set of solvation radii for Li and O to model the solvation of lithium superoxide, peroxide, and oxide species. The absolute solvation free energies of Li^+ (−122.7 kcal/mol) and O_2^- (−75.8 kcal/mol) in acetonitrile were derived from the available literature data [33, 49–54], as described in Sect. 3. These values were used to refit the default Li and O solvation radii from $r_{Li} = 1.226$ and $r_O = 1.600$ Å to $r_{Li} = 1.333$ and $r_O = 1.797$ Å. Using the fitted radii within the dielectric continuum model decreased the absolute solvation free energies of various lithium–oxygen species by 8–20 kcal/mol. In contrast, the sensitivity of solvation calculations to the choice of Li and O solvation radii for the explicitly solvated $Li_xO_y(CH_3CN)_n$ clusters is <1.0 kcal/mol for $n = 4$ and <0.03 kcal/mol for $n = 8$ (at $n = 8$ the solute is fully surrounded by explicit solvent molecules). The surface-area dependent nonpolar solvation contributions were not included in the calculation of solvation free energies using mixed cluster/continuum models, because the difference in these terms (Eq. 1) for solvent and solute–solvent clusters with the same n is relatively small (e.g., 0.28 kcal/mol for O_2^- and 0.77 kcal/mol for Li_2O_2 at $n = 8$).

2.4 Conformational sampling of solvent and solute–solvent clusters

We carried out a search of the low-energy conformers of $(CH_3CN)_n$ and $X(CH_3CN)_n$ ($X = Li^+$, O_2^-, LiO_2, Li_2O_2, LiO, Li_2O; $n = 4$–10). For clusters with $n = 4$, a thorough systematic search of the plausible low-energy structures was performed. For clusters with $n = 6$, 8, and 10, we used the excluded-volume constrain method with Monte Carlo sampling (BLENDS) to generate 30–40 initial cluster configurations [55, 56]. The initial structures were subjected to full geometry optimization at the B3LYP/6-31G^{**} level, followed by single point energy calculations at the M06-L/6-311++G^{**} level. These were combined with the solvation free energies computed at the B3LYP/6-311++G^{**} level to yield the final ranking of the complexes. Some initial configurations were also built upon visual inspection and conformational rearrangement of the optimized clusters. Additional calculations for $(CH_3CN)_n$ and $O_2^-(CH_3CN)_n$ ($n = 6, 8$) were performed using geometries optimized at the M06-L/6-31G^{**} level. Solvation calculations (Eq. 1) were reported using the lowest-energy clusters in solution. The Boltzmann averaging did not lead to significant changes in the solvation free energies calculated using Eq. 1 (<1.0 kcal/mol) and therefore was not included.

3 Absolute solvation free energies of Li^+ and O_2^- in acetonitrile

Direct experimental measurements can only provide relative values for the solvation free energies of ions. These are often tabulated with respect to the solvation free energy of the proton, which can be derived by applying an appropriate extra-thermodynamic assumption [57]. Thus, the accurate estimation of the absolute solvation free energy of the proton is of fundamental importance and has been the subject of numerous theoretical and experimental studies [57–65]. Several researchers in recent publications [27, 45, 57, 63–65] advocated using solvation free energies of ions on the basis of the cluster pair approximation, and we follow this recommendation in the present study.

3.1 $\Delta G^*_{solv}(Li^+)$

The solvation free energy of the proton in acetonitrile determined by Kelly et al. [33] using the cluster pair approximation is $\Delta G^*_{solv}(H^+) = -260.2$ kcal/mol. Absolute solvation free energies for a series of ions were determined based on this value, but no data were reported for Li^+ and O_2^-. Gibbs free energies of transfer of ions

from water to organic solvents were reviewed by Marcus et al. [49, 50]. The recommended value for transfer of Li^+ from water to acetonitrile provided by Marcus [49] is 6.8 kcal/mol. It is based on the reference electrolyte assumption using the tetraphenylarsonium tetraphenylborate salt to split the total solvation free energy evenly between its cation and anion. A comparison of Gibbs free energies of transfer of Na^+, K^+, Cs^+, Ag^+, and Cl^- from water to acetonitrile in the compilations of Marcus et al. [49] (classified as recommended values) and Kelly et al. [33] shows that the values by Kelly et al. [33] are on average 1.1 kcal/mol lower. With this correction and $\Delta G^*_{solv}(Li^+) = -128.4$ kcal/mol in water, our best estimate of the $\Delta G^*_{solv}(Li^+)$ in acetonitrile is −122.7 kcal/mol.

3.2 $\Delta G^*_{solv}(O_2^-)$

The solvation free energy of superoxide anion in acetonitrile can be determined from the reported reversible one-electron reduction potential of O_2. The measured reduction potential of oxygen is −1.235 V against the ferrocenium/ferrocene (Fc^+/Fc) redox couple [51]. Using the recommended literature conversion constants [52] from the Fc^+/Fc scale in acetonitrile to the standard hydrogen electrode scale (SHE, 0.624 V) and from the SHE reference to the Li^+/Li reference in acetonitrile solutions (2.793 V) gives the value of the O_2/O_2^- potentials in acetonitrile to be −0.611 and 2.182 V versus SHE and Li^+/Li electrode, respectively. This is in good agreement with the value of −0.63 V versus SHE given in Ref. [53].

Through the use of the thermodynamic cycle shown in Scheme 2, the absolute solvation free energy of O_2^- can be written as

$$\Delta G^*_{solv}\left(O_2^-\right) = -\Delta_f G^o_{298}[Li^+(g)] - \Delta_f G^o_{298}[O_2^-(g)] - FE^* - \Delta G^*_{solv}(Li^+) - 2\Delta G^{o\to *}, \quad (2)$$

where $\Delta_f G^o_{298}[Li^+(g)]$ and $\Delta_f G^o_{298}[O_2^-(g)]$ are the standard gas-phase free energies of formation of Li^+ and O_2^-, respectively, F is Faraday's constant, E^* is the standard reduction potential versus Li^+/Li, and $\Delta G^{o\to *}_{solv} = 1.89$ kcal/mol ($T = 298.15$ K) is the standard state correction defined in Sect. 2.1. Substituting the tabulated values for the gas-phase free energies of formation of Li^+ (154.59 kcal/mol) [54] and O_2^- (−10.24 kcal/mol) [54] into Eq. 2, together with the values of E^*, $\Delta G^*_{solv}(Li^+)$, and $\Delta G^*_{solv}(Li^+)$ determined above, we obtain the value of −75.7 kcal/mol for the absolute solvation free energy of O_2^- in acetonitrile. For comparison, the experimental value in water is −83.3 kcal/mol [63]. The difference of 7.6 kcal/mol is much larger than that explained from a simple change in the medium's dielectric constant (1.3 kcal/mol), if the O solvation radius is kept constant.

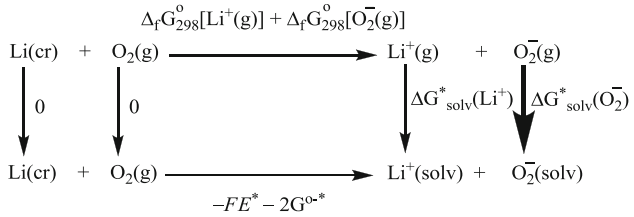

Scheme 2 Thermodynamic cycle for the calculation of $\Delta G^*_{solv}(O_2^-)$

4 Results and discussion

4.1 The accuracy of DFT calculations in the gas phase

First, we examine the performance of several DFT methods in predicting the experimental [66–70] enthalpies ($\Delta H_{0K,r}$) and standard Gibbs free energies ($\Delta G^o_{g,r}$) for the complexation of small ions with several acetonitrile and ether-based ligands in the gas phase. Table 1 compares the performance of the B3LYP, M06, M06-2X, and M06-L density functionals using different basis sets and DFT optimized geometries. B3LYP functional is chosen given its widespread use and that it provides reasonable geometries for metal ion-ligand complexes [71, 72]. M06 family of density functionals is selected because of its excellent performance on non-covalent interactions [39, 40] including water and ion-water clusters [73].

The accuracy of each method is characterized by the mean unsigned error (MUE) listed in the last two columns of Table 1. Utilizing a 6-311++G^{**} basis set, the MUE for $\Delta G^o_{g,r}$ sorted in increasing order is 1.18 (M06-L), 1.55 (M06), 4.5 (M06-2X), and 5.0 (B3LYP) kcal/mol. Further improvement in accuracy for the M06-class of density functionals can be achieved by performing single point energy calculations on B3LYP optimized geometries or using more extended basis sets. The approach of calculating M06 energies on B3LYP geometries was first introduced by Truhlar [74] and later found to give good agreement with experiment in describing the relative stability of organometallic complexes [71, 72]. We find that the M06-L/6-311++G^{**}//B3LYP/6-311++G^{**} method with the MUE of 1.93 kcal/mol for $\Delta H_{0K,r}$ and 0.26 kcal/mol for $\Delta G^o_{g,r}$ shows the best overall performance. Using M06-L/aug-cc-pVTZ single-point energies on M06-L/6-311++G^{**} optimized geometries with the MUE of 2.10 kcal/mol for $\Delta H_{0K,r}$ and 0.39 kcal/mol for $\Delta G^o_{g,r}$ gives the second best performance. The accuracy of the M06-L functional to reproduce the gas-phase complexation free energies is impressive. The best DFT methods as ranked by

Table 1 Comparison of the experimental enthalpies ($T = 0$ K) and standard Gibbs free energies ($T = 298.15$ K) of complexation in the gas phase to those obtained with various DFT methods (kcal/mol)

Methods	$O_2^- + 4MeCN = O_2^-(MeCN)_4$		$Na^+ + 4MeCN = Na^+(MeCN)_4$		$Na^+ + 3EtOEt = Na^+(EtOEt)_3$		$Li^+ + 4MeOMe = Li^+(MeOMe)_4$		Mean unsigned error	
	$\Delta H_{0K,r}$	$\Delta G^o_{g,r}$	$\Delta H_{0K,r}$	$\Delta G^o_{g,r}$	$\Delta H_{0K,r}$	$\Delta G^o_{g,r}$	$\Delta H_{0K,r}$	$\Delta G^o_{g,r}$	$\Delta H_{0K,r}$	$\Delta G^o_{g,r}$
Expt	−53.1[a]	−26.2[a]	−91.45[b]	−61.75[b]	−71.2[c]	−44.6[c]	−105.7[d]			
B3LYP/6-311++G^{**}	−50.14	−18.23	−93.74	−65.68	−68.95	−41.45	−105.09	−70.60	2.03	5.02
B3LYP/aug-cc-pVTZ[e]	−48.73	−16.82	−93.70	−65.65	−67.21	−39.71	−101.40	−66.91	3.73	6.05
M06/6-311++G^{**}	−59.17	−27.26	−90.67	−62.61	−74.82	−47.32	−108.20	−73.71	3.24	1.55
M06-2X/6-311++G^{**}	−58.66	−26.75	−94.64	−66.59	−80.29	−52.79	−116.91	−82.42	7.26	4.52
M06-L/6-311++G^{**}	−60.51	−28.61	−90.39	−62.34	−72.66	−45.16	−105.45	−70.96	2.54	1.18
M06-L/aug-cc-pVTZ[f]	−58.35	−26.44	−90.66	−62.60	−72.04	−44.54	−104.16	−69.67	2.1	0.39
M06//B3LYP/6-311++G^{**}	−56.94	−25.03	−90.59	−62.53	−73.03	−45.53	−108.05	−73.57	2.22	0.96
M06-2X//B3LYP/6-311++G^{**}	−56.03	−24.13	−94.56	−66.51	−78.40	−50.90	−115.93	−81.44	5.87	4.38
M06-L//B3LYP/6-311++G^{**}	**−58.17**	**−26.27**	**−90.36**	**−62.31**	**−71.93**	**−44.44**	**−104.90**	**−70.41**	**1.93**	**0.26**

Geometries are optimized using the 6-311G++G^{**} basis set. Harmonic frequency analysis is performed at the B3LYP/6-31G^{**} level. The results obtained with the M06-L//B3LYP method (M06-L single point energies on B3LYP optimized geometries) have the lowest mean unsigned error and are shown in bold

[a] Ref. [66]

[b] The average of two values taken form Refs. [67] and [68]

[c] Ref. [69]

[d] Ref. [70]

[e] B3LYP/aug-pVTZ single-point energies on B3LYP/6-311++G^{**} optimized geometries

[f] M06-L/aug-pVTZ single-point energies on M06-L/6-311++G^{**} optimized geometries

their overall performance are utilized for the calculation of the complexation and solvation free energies of charged and ionic solutes in acetonitrile.

4.2 The accuracy of solvation calculations in acetonitrile using a Poisson–Boltzmann continuum solvent model

Next, we test the ability of the PB continuum model in Jaguar to reproduce the solvation free energies of neutral organic solutes in acetonitrile. The nonelectrostatic part of the solvation free energy was approximated by the solvent-accessible surface area (SASA) dependent term [75] fitted to minimize the deviation between the measured and calculated solvation free energies

$$\Delta G^*_{solv} = \Delta G^{elec}_{solv} + a \cdot \mathrm{SASA}, \quad (3)$$

where a is a fitting parameter.

Table 2 summarizes the performance of the three solvation models against the experimental data [43], as gauged by the mean square (rms) deviation. Using the default solute van der Waals radii in Jaguar leads to a systematic overestimation of ΔG^{elec}_{solv} for polar solutes. In this case, the rms deviation cannot be significantly improved by the least square fitting of the SASA term. The agreement with experiment can be greatly improved by optimizing the solute van der Waals radii for a given solvent. Due to a limited amount of available experimental data for neutral solutes in acetonitrile [43], we chose to optimize a single scaling parameter for all atomic radii. Using the optimized scaling factor of 1.4 together with the SASA dependent energy term gives almost a five-fold improvement in accuracy over the default parameters choice. This approach compares favorably in accuracy with the SM8 solvation model [43, 44] that has been extensively parameterized for many organic solvents.

Furthermore, we demonstrate that our computational methodology is capable of predicting the complexation behavior of lithium ion in acetonitrile. Figure 1 shows the comparison of the computed and experimental [76]

Table 2 Calculated and experimental solvation free energies (ΔG^*_{solv}) of neutral solutes in acetonitrile (kcal/mol)

Solute/rmsd	Default[a]	Scaled[b]	SM8[c]	Expt[d]
Acetonitrile	−8.72	−5.77	−6.37	−4.85
1,4-Dioxane	−6.79	−4.53	−4.76	−5.33
2-Butanone	−6.30	−5.07	−5.64	−4.73
Ethanol	−6.40	−4.07	−4.22	−4.43
Nitromethane	−9.02	−5.78	−5.77	−5.62
Toluene	−2.67	−4.06	−5.23	−4.68
n-Octane	0.74	−4.06	−3.81	−3.57
Rms deviation	2.87	0.58	0.75	

ΔG^*_{solv} is calculated as a sum of the electrostatic solvation free energy (ΔG^{elec}_{solv}) computed by Jaguar and the nonelectrostatic component obtained from the least-square fitting to the solvent-accesible surface area (SASA), $\Delta G^*_{solv} = \Delta G^{elec}_{solv} + a{\cdot}SASA$

[a] The default solute van der Waals radii in Jaguar

[b] van der Waals radii scaled by a factor of 1.4, chosen to minimize the rms deviation

[c] The SM8 solvation model in Jaguar used in conjunction with the M06/6-31G^* method

[d] Ref. [43]

complexation free energies of lithium ion with other aprotic solvents (1:1 stoichiometry) in acetonitrile. The complexation is modeled as ligand exchange between the first tetrahedral shell (treated explicitly) and the outer coordination shell around the lithium ion

$$[Li(CH_3CN)_4]^+ + \text{solvent} = [Li(CH_3CN)_3(\text{solvent})]^+ + CH_3CN \quad (4)$$

DFT calculations are carried out at the M06-L/6-311++G^{**}//B3LYP/6-311++G^{**} level, which provides the most accurate gas-phase complexation free energies (Sect. 4.1). Solvation effects beyond the first solvation shell are calculated using a PB continuum solvent model with the default and optimized (scaled by 1.4) solute van der Waals radii and the SM8 solvation model.

Figure 1 reveals that our theoretical predictions agree very closely with experimental measurements (the rms deviation is 0.87 kcal/mol) when the optimized solute radii are used. If, however, the default solute radii are employed, the rms deviation is increased almost three times (2.59 kcal/mol), which is only marginally lower than that given by gas-phase calculations (2.89 kcal/mol). This strongly supports our simple protocol of scaling the atomic radii to improve the accuracy of implicit solvation calculations. In contrast, application of the SM8 solvation model at the M06/6-31G^* level with partial atomic charges calculated using the CM4M model does not improve the agreement with experiment [76] when compared to the results obtained with no implicit solvation.

4.3 Calculation of solvation free energies of Li^+ and O_2^- in acetonitrile

The solvation free energies of charged solutes are calculated using the cluster cycle shown in Scheme 1. The most important solute–solvent interactions are included explicitly into the quantum chemical model, while the rest of the solvent is approximated by the dielectric continuum model. Explicit modeling of the first solvation shell for neutral and singly charged solutes should be sufficient to give a satisfactory description of their thermodynamic [28] and complexation [77] properties in solution (see Sect. 4.2). Indeed, excellent agreement between the calculated and experimental solvation free energies of Li^+ and O_2^- in acetonitrile is found by including the full first solvation shell around these ions (Table 3). Consistent with these results, no significant variation in the calculated $\Delta G^*_{solv}(Li_2O_2)$ is observed when the number of solvent molecules is extended beyond the first solvation shell (see Sect. 4.4). Conversely, previous studies have shown that more extended solvation layers are required for an adequate description of doubly and more highly charge ions [28, 77].

The Li^+ ion displays tetrahedral coordination geometry in bulk solution [78]. Calculations for the 4-, 5-, and 6-

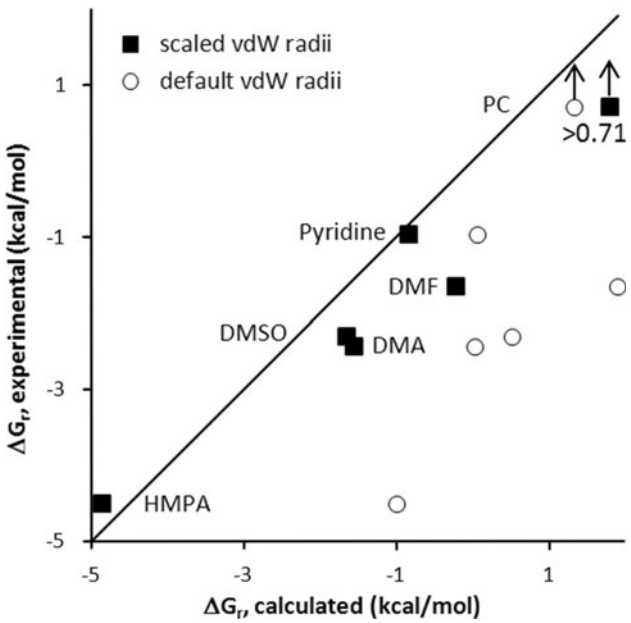

Fig. 1 Complexation free energies of lithium ion in acetonitrile with one molecule of HMPA (hexamethylphosphoramide), DMA (dimethylacetamide), DMSO (dimethyl sulfoxide), DMF (dimethylformamide), pyridine, and PC (propylene carbonate). Experimental complexation free energies were taken from Ref. [76]. Calculations were carried out for the model reaction (4) at the M06-L/6-311++G^{**}//B3LYP/6-311++G^{**} level. Solvation effects beyond the first solvation shell were treated with a dielectric continuum model using the default and scaled (by 1.4) van der Waals radii (see Table 2)

Table 3 Solvation free energies of the Li^+ and O_2^- ions in acetonitrile calculated using the thermodynamic cycle shown in Scheme 1 (kcal/mol)

n	$\Delta G^*_{solv}(Li^+)$			$\Delta G^*_{solv}(O_2^-)$		
	Method I[a]	Method II[b]	Expt[c]	Method I[a]	Method II[b]	Expt[c]
4	−123.9	−125.8		−70.0	−70.0	
6				−71.7	−74.4	
8				−74.4	−73.8	
Bulk limit			−122.7			−75.8

[a] M06-L/6-311++G^{**} single point energies on B3LYP/6-311++G^{**} ($n = 4$) or B3LYP/6-31G^{**} optimized geometries. Solvation effects are included at the B3LYP/6-311G++(d,p) level

[b] M06-L/aug-cc-pVTZ single point energies on M06-L/6-311++G^{**} ($n = 4$) or M06-L/6-31G^{**} optimized geometries. Solvation effects are included at the M06-L/6-311++G^{**} level

[c] See Sect. 3

coordinate $Li^+(CH_3CN)_6$ complexes in the gas phase confirm that the most energetically favorable position for the fifth or sixth solvent molecules is in the second solvation shell, where a lone pair of nitrogen is directed toward the hydrogen atom of the adjacent solvent molecule in the first coordination shell (Fig. 2). The 5- and 6-coordinate conformations are 0.5–0.7 kcal/mol higher in energy at the M06-L level. Additional C–H···N interactions with the solvent molecules in the second shell will be able to provide much stronger stabilization of the four-coordinate geometry in the bulk limit.

Structures of the most stable $(CH_3CN)_n$ and $O_2^-(CH_3CN)_n$ complexes ($n = 4$, 6, 8) with inclusion of the solvent reaction field are shown in Fig. 3. The lowest energy acetonitrile tetramer at the M06-L level is arranged in a 3-D conformation, where two dimer units in each layer are rotated 90° from each other. In agreement with previous results [79], a cyclic ring structure is favored at the B3LYP level. The lowest energy hexamer and octamer clusters are formed by stacking the dimers in different layers. Not surprisingly, acetonitrile molecules in $O_2^-(CH_3CN)_n$ clusters are oriented to maximize their interaction with the superoxide anion-radical. For example, each oxygen atom in $O_2^-(CH_3CN)_8$ is coordinated by four acetonitrile molecules, which is the maximum coordination number for the OH^- oxygen in aqueous solution [80].

Table 3 shows a comparison of the calculated and experimentally derived (Sect. 3) solvation free energies of Li^+ and O_2^- in acetonitrile. Calculations are performed at the M06-L level using B3LYP (method I) and M06-L (method II) optimized geometries, which provides the best overall performance for ion complexation in the gas phase (Table 1). The use of a cluster model with four ligands in the coordination shell gives the calculated free energy of Li^+ that is in excellent agreement with the experimental value. For O_2^-, the calculated ΔG^*_{solv} value exhibits a systematic dependence on cluster size, increasing by 3.8–4.4 kcal/mol from $n = 4$–8. This shows that a complete saturation of the first solvation shell is needed to obtain reasonably converged results in solution. With an inclusion of a full first solvation shell ($n = 8$), the calculated $\Delta G^*_{solv}(O_2^-)$ agrees closely with the experimental value. Comparison of the two computational methods in Table 3 does not reveal significant difference in their performance. In both cases, the results are within the experimental uncertainty [33, 63] of at least ±2 kcal/mol. Given that fact, subsequent solvation free energy calculations were based on the optimized cluster geometries obtained with

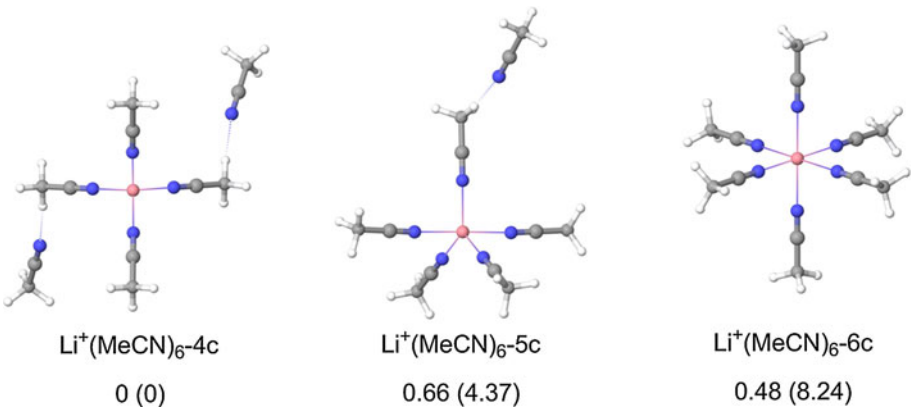

Fig. 2 Structures and relative electronic energies of $Li^+(MeCN)_6$ in the gas phase (kcal/mol) obtained at the M06-L/6-311++G^{**}//B3LYP/6-31G^{**} level of theory. Relative energies obtained at the B3LYP/6-311++G^{**}//B3LYP/6-31G^{**} level are shown in *parentheses*

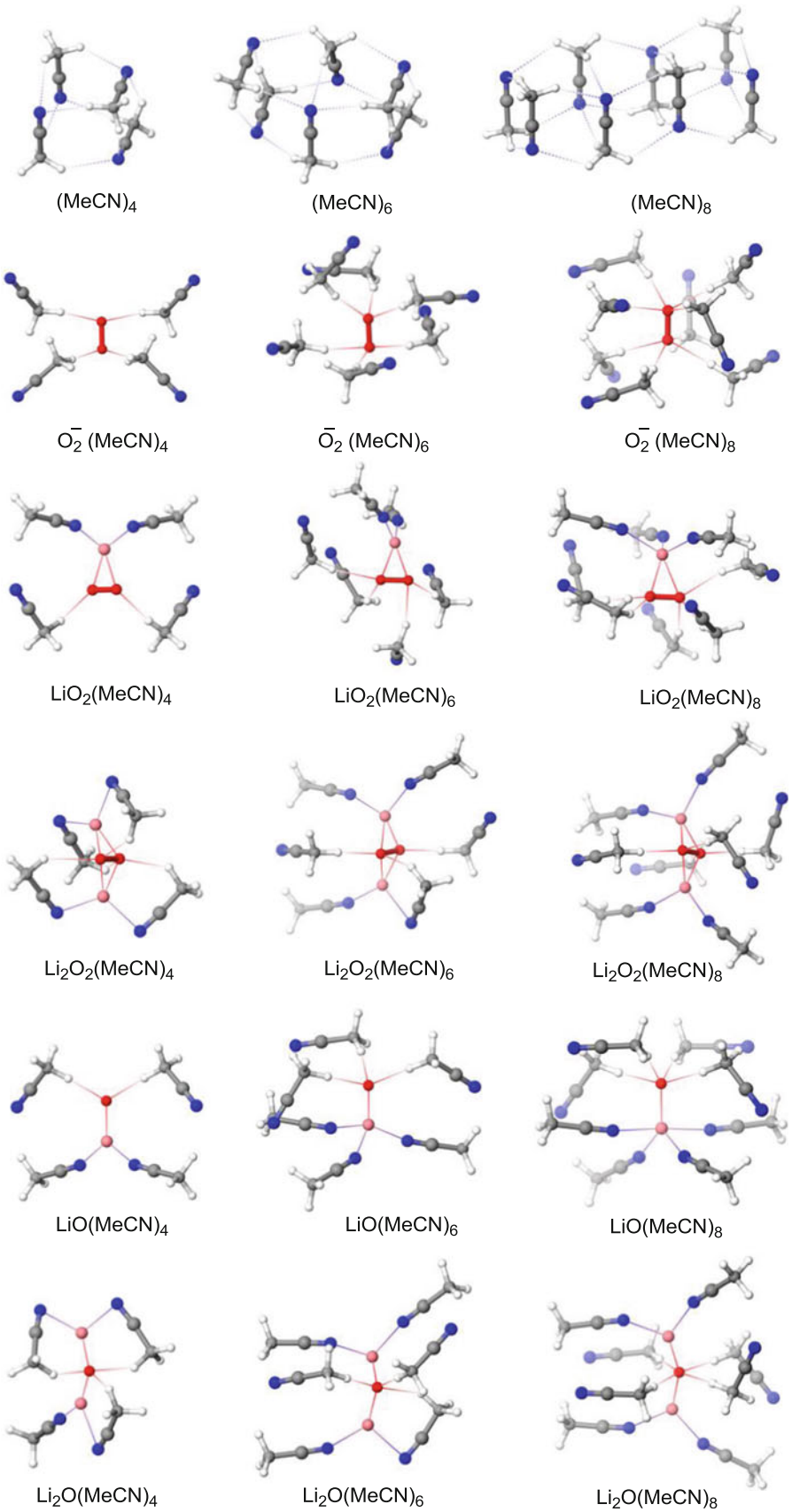

Fig. 3 Structures of $(MeCN)_n$ and $X(MeCN)_n$ clusters ($X = O_2^-$, LiO_2, Li_2O_2, LiO, and Li_2O; $n = 4$–8) optimized at the B3LYP/6-311++G^{**} ($n = 4$) or B3LYP/6-31G^{**} ($n = 6$, 8) level

Table 4 Solvation free energies of LiO_2, Li_2O_2, LiO, and Li_2O in acetonitrile calculated using the thermodynamic cycle shown in Scheme 1 (kcal/mol) and the pure dielectric continuum model

n	LiO_2	Li_2O_2	LiO	Li_2O
0 (default)[a]	−39.4 (−42.9)	−58.4 (−64.2)	−51.7 (−55.0)	−74.4 (−81.2)
0 (fitted)[b]	−31.2 (−33.9)	−43.3 (−46.8)	−41.6 (−43.9)	−54.6 (−58.3)
4	−28.2	−28.9	−35.0	−39.1
6	−29.1	−38.6	−40.1	−48.8
8	−32.7	−43.5	−41.9	−56.7
10		−42.6		

[a] The default solute van der Waals radii in Jaguar ($r_{Li} = 1.226$ and $r_O = 1.600$ Å). The results are shown for both gas-phase and solvent-optimized (in parenthesis) geometries

[b] van der Waals radii of Li and O fitted to reproduce the experimental solvation free energies of Li^+ and O_2^- in acetonitrile ($r_{Li} = 1.333$ and $r_O = 1.797$ Å). The results are shown for both gas-phase and solvent-optimized (in parenthesis) geometries

the computationally less expensive B3LYP method (method I in Table 3).

4.4 Calculation of solvation free energies of LiO_2, Li_2O_2, LiO, and Li_2O in acetonitrile

Figure 3 shows the structures of the most stable $X(CH_3CN)_n$ complexes in acetonitrile with $X = LiO_2$, Li_2O_2, LiO, and Li_2O and coordination number $n = 4$, 6, and 8. These structures are used to calculate the solvation free energies of ionic solutes X in acetonitrile as a function of n (Table 4). The calculated solvation free energies of all lithium–oxygen species increase monotonically in absolute value as n increases from $n = 4$–8. The results indicate that the rate of the convergence of $\Delta G^*_{solv}(X)$ with cluster size depends strongly on the polarity of a neutral solute X. The change in $\Delta G^*_{solv}(X)$ with $n = 4$–8 varies from 4.5 kcal/mol for LiO_2 to 17.6 kcal/mol for Li_2O. In contrast, a much smaller variation in $\Delta G^*_{solv}(Li_2O_2)$ is observed from $n = 8$ to 10 (0.9 kcal/mol). This may not be surprising since the first solvation shell around Li_2O_2 is fully saturated at $n = 8$ and the additional solvent molecules in the second shell are not expected to significantly impact the calculated ΔG^*_{solv} for neutral and monocharged solutes [28, 77]. Thus, inclusion of a complete first solvation shell around neutral lithium–oxygen solutes should be sufficient for adequate prediction of their solvation free energies.

Table 4 also summarizes the solvation free energies of neutral Li_xO_y solutes computed using a pure dielectric continuum model in Jaguar. As expected, the results of calculations are highly sensitive to the choice of the solute atomic radii that define the dielectric continuum boundary. In this work, the default solute radii of Li and O are tuned to reproduce the experimental solvation free energies of Li^+ and O_2^- in acetonitrile. With this change, the difference in the calculated ΔG^*_{solv} for Li_2O_2 and Li_2O could be as large as 15–20 kcal/mol. The important question arises as to whether the solvation thermodynamics of Li_xO_y compounds with oxygen in variable oxidation states (−0.5, −1, −2) can be accurately described by a single set of Li and O atomic radii. A comparison with converged results using mixed cluster/continuum models indicates that implicit solvation calculations employing the fitted solute radii (optimized for Li^+ and O_2^-) are able to accurately reproduce the solvation free energies of lithium superoxide, peroxide, monoxide, and oxide. The mean unsigned error is 1.0 and 2.0 kcal/mol for gas-phase and solvent-optimized geometries, respectively. Given excellent agreement with experiment for $\Delta G^*_{solv}(Li^+)$ and $\Delta G^*_{solv}(O_2^-)$ in acetonitrile, the atomic radii for solvents where no experimental data are available can be derived from first principles using mixed cluster/continuum calculations. Broad transferability of these parameters, as illustrated for acetonitrile, will provide a useful framework to estimate the effect of a solvent on the thermodynamics of the elementary reaction steps involved in ORR and OER [19–23].

As a final note, solvation calculations assume no solvent involvement in the reaction with a solute. However, in several instances we observed a spontaneous proton transfer from one of the solvent molecules to the oxygen atom of Li_2O, leading to the formation of LiOH as a more stable product (Fig. 4). This observation indicates that many organic solvents may be intrinsically unstable in the presence of molecular Li_2O, thereby suggesting that the formation of Li_2O in the organic electrolyte rechargeable Li-air battery should be avoided.

5 Conclusions

Solvent influences the thermodynamic stability of reaction intermediates and plays a decisive role in determining the discharge/charge characteristics of the non-aqueous rechargeable lithium-air battery. In this work, we employed a mixed cluster/continuum model with varying number of explicit solvent molecules (n) to calculate the solvation free

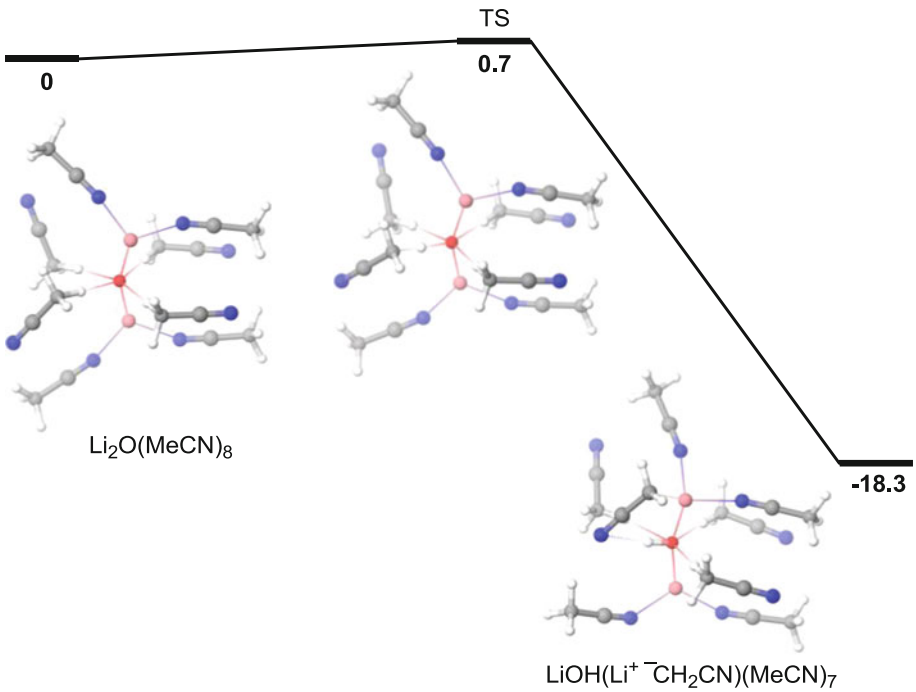

Fig. 4 Reaction free energy profile ($T = 298.15$ K) for proton transfer by Li_2O from the methyl group of acetonitrile (kcal/mol). Solvent effects are modeled by explicit inclusion of eight acetonitrile molecules in the first solvation shell and treatment of the rest of the solvent with a dielectric continuum model using the scaled (by 1.4) van der Waals radii

energies of charged Li^+ and O_2^- and neutral LiO_2, Li_2O_2, LiO, and Li_2O solutes in acetonitrile solvent. Calculations were performed using the M06-L density functional that gives the best performance for gas-phase complexation free energies and a Poisson-Boltzmann continuum model with atomic radii optimized for neutral solutes. We find that using clusters with a fully saturated first solvation shell gives solvation free energies of Li^+ and O_2^- that are in excellent agreement with the experimental values derived from studies on ion–solvent clusters. Mixed cluster/continuum calculations on various lithium–oxygen species enable us to evaluate the performance of pure continuum solvent models. Using a single set of Li and O atomic radii fitted to reproduce the solvation free energies of Li^+ and O_2^- within a conventional dielectric continuum approximation shows excellent performance in reproducing the solvation free energies of LiO_2, Li_2O_2, LiO, and LiO_2 with oxygen across multiple oxidation states. This allows one to include solvent effects in the theoretical models of the elementary reaction steps of oxygen reduction and evolution in the aprotic electrolyte Li-air battery using a single set of solvation parameters within the framework of continuum solvation models. In a broad context, this study shows that with a choice of the accurate density functional for non-covalent interactions, implicit solvation model optimized for a given solvent, and explicit consideration of the most important solute–solvent interactions, theoretical models can provide reliable description of solvation thermodynamics and complexation of charged and highly ionic solutes in organic solvents.

Acknowledgments I am indebted to Dr. Mario Blanco for providing me with the algorithm for sampling the initial configurations of solvated clusters. This work was supported by Liox Power, Inc., Pasadena, CA.

References

1. Laoire CO, Mukerjee S, Abraham KM, Plichta EJ, Hendrickson MA (2010) J Phys Chem C 114:9178–9186
2. Girishkumar G, McCloskey BD, Luntz A, Swanson S, Wilcke W (2010) J Phys Chem Lett 1:2193–2203
3. Bruce PG, Freunberger SA, Hardwick LJ, Tarascon JM (2012) Nat Mater 11:19–29
4. Christensen J, Albertus P, Sanchez-Carrera RS, Lohmann T, Kozinsky B, Liedtke R, Ahmed J, Kojic A (2012) J Electrochem Soc 159:R1–R30
5. Bryantsev VS, Blanco M (2011) J Phys Chem Lett 2:379–383
6. Freunberger SA, Chen Y, Peng Z, Griffin JM, Hardwick LJ, Bardé F, Novák P, Bruce P (2011) J Am Chem Soc 133:8040–8047
7. Mizuno F, Nakanishi S, Kotani Y, Yokoishi S, Iba H (2010) Electrochemistry 78:403–405
8. McCloskey BD, Bethune DS, Shelby RM, Girishkumar G, Luntz AC (2011) J Phys Chem Lett 2:1161–1166
9. McCloskey BD, Scheffler R, Speidel A, Bethune DS, Shelby RM, Luntz AC (2011) J Am Chem Soc 133:18038–18041
10. Xiao J, Hu J, Wang D, Hu D, Xu W, Graff GL, Nie Z, Liu J, Zhang JG (2011) J Power Sources 196:5674–5678
11. Veith GM, Dudney NJ, Howe J, Nanda J (2011) J Phys Chem C 115:14325–14333
12. Wang H, Xie K (2012) Electrochim Acta 64:29–34
13. Freunberger SA, Chen Y, Drewett NE, Hardwick LJ, Bardé F, Bruce PG (2011) Angew Chem Int Ed 50:8609–8613
14. Chen Y, Freunberger SA, Peng Z, Bardé F, Bruce PG (2012) J Am Chem Soc 134:7952–7957

15. Bryantsev VS, Giordani V, Walker W, Blanco M, Zecevic S, Uddin J, Addison D, Chase GV (2011) J Phys Chem A 115:12399–12409
16. Mizuno F, Nakanishi S, Shirasawa A, Takechi K, Shiga T, Nishikoori H, Iba H (2011) Electrochemistry 79:876–881
17. Zhang Z, Lu J, Assary RS, Du P, Wang HH, Sun YK, Qin Y, Lau KC, Greeley J, Redfern PC (2011) J Phys Chem C 115:25535–25542
18. Crowther O, Meyer B, Solomon M (2011) Electrochem Solid St Lett 14:A113–A115
19. Hummelshøj JS, Blomqvist J, Datta S, Vegge T, Rossmeisl J, Thygesen KS, Luntz AC, Jacobsen KW, Nørskov JK (2010) J Chem Phys 132:071101-1–071101-4
20. Viswanathan V, Thygesen KS, Hummelshøj JS, Nørskov JK, Girishkumar G, McCloskey BD, Luntz AC (2011) J Chem Phys 135:214704-1–214704-10
21. Xu Y, Shelton WA (2011) J Electrochem Soc 158:A1177–A1184
22. Mo Y, Ong SP, Ceder G (2011) Phys Rev B 84:205446-1–205446-9
23. Radin MD, Rodriguez JF, Tian F, Siegel DJ (2012) J Am Chem Soc 134:1093–1103
24. Wasileski SA, Janik MJ (2008) Phys Chem Chem Phys 10:3613–3627
25. Janik MJ, Taylor CD, Neurock M (2009) J Electrochem Soc 156:B126–B135
26. Rossmeisl J, Skúlason E, Björketun ME, Tripkovic V, Nørskov JK (2008) Chem Phys Lett 466:68–71
27. Warren GL, Patel SJ (2007) Chem Phys 127:064509-1–064509-19
28. Bryantsev VS, Diallo MS, Goddard WA III (2008) J Phys Chem B 112:9709–9719
29. Pliego JR Jr (2011) Theor Chem Acc 128:275–283
30. Merchant S, Dixit PD, Dean KR, Asthagiri DJ (2011) Chem Phys 135:054505-1–054505-8
31. Ziegler MJ, Madura JD (2011) J Solution Chem 40:1383–1398
32. Peng Z, Freunberger SA, Hardwick LJ, Chen Y, Giordani V, Bardé F, Novák P, Graham D, Tarascon JM, Bruce PG (2011) Angew Chem Int Ed 50:6351–6355
33. Kelly CP, Cramer CJ, Truhlar DG (2007) J Phys Chem B 111:408–422
34. Jaguar, version 7.7 (2010) Schrödinger, LLC, New York
35. Bylaska EJ, de Jong WA, Govind N, Kowalski K, Straatsma TP, Valiev M, Wang D, Apra E, Windus TL, Hammond J, Nichols P, Hirata S, Hackler MT, Zhao Y, Fan PD, Harrison RJ, Dupuis M, Smith DMA, Nieplocha J, Tipparaju V, Krishnan M, Wu Q, Van Voorhis T, Auer AA, Nooijen M, Brown E, Cisneros G, Fann GI, Fruchtl H, Garza J, Hirao K, Kendall R, Nichols JA, Tsemekhman K, Wolinski K, Anchell J, Bernholdt D, Borowski P, Clark T, Clerc D, Dachsel H, Deegan M, Dyall K, Elwood D, Glendening E, Gutowski M, Hess A, Jaffe J, Johnson B, Ju J, Kobayashi R, Kutteh R, Lin Z, Littlefield R, Long X, Meng B, Nakajima T, Niu S, Pollack L, Rosing M, Sandrone G, Stave M, Taylor H, Thomas G, van Lenthe J, Wong A, Zhang Z (2008) NWChem, a computational chemistry package for parallel computers, version 5.1.1. Pacific Northwest National Laboratory, Richland
36. Kendall RA, Aprà E, Bernholdt DE, Bylaska EJ, Dupuis M, Fann GI, Harrison RJ, Ju J, Nichols JA, Nieplocha J, Straatsma T, Windus TL, Wong AT (2000) Comput Phys Commun 128:260–283
37. Becke AD (1988) Phys Rev A 38:3098–3100
38. Lee CT, Yang WT, Parr RG (1988) Phys Rev B 37:785–789
39. Zhao Y, Truhlar DG (2006) J Chem Phys 125:194101-1–194101-17
40. Zhao Y, Truhlar DG (2008) Theor Chem Acc 120:215–241
41. Dunning TH Jr (1989) J Chem Phys 90:1007–1023
42. Kendall RA, Dunning TH Jr (1992) J Chem Phys 96:6796–6806
43. Marenich AV, Olson RM, Kelly CP, Cramer CJ, Truhlar DG (2007) J Chem Theory Comput 3:2011–2033
44. Cramer CJ, Truhlar DJ (2008) Acc Chem Res 41:760–768
45. Zuo CS, Wiest O, Wu YD (2009) J Phys Chem A 113:12028–12034
46. Barone V, Cossi M, Tomasi J (1997) J Chem Phys 107:3210–3221
47. Mennucci B, Tomasi J (1997) J Chem Phys 107:3032–3041
48. Rappé AK, Casewit CJ, Colwell KS, Goddard WA III, Skiff WM (1994) J Am Chem Soc 116:11875–11882
49. Kalidas C, Hefter G, Marcus Y (2000) Chem Rev 100:819–852
50. Marcus Y (2007) Chem Rev 107:3880–3897
51. Vasudevan D, Wendt HJ (1995) Electroanalyt Chem 192:69–74
52. Pavlishchuk VV, Addison AW (2000) Inorg Chim Acta 298:97–102
53. Song C, Zhang J (2008) In: Zhang J (ed) PEM fuel cell electrocatalysts and catalyst layers: fundamentals and applications. Springer, London
54. NIST Chemistry Webbook (2005) http://webbook.nist.gov/chemistry/
55. Blanco MJ (1991) Comput Chem 12:237–247
56. Fan CF, Olafson BD, Blanco M, Hsu SL (1992) Macromolecules 25:3667–3676
57. Hünenberger P, Reif M (2011) Single-ion solvation: experimental and theoretical approaches to elusive thermodynamic quantities. RSC, Cambridge
58. Marcus Y (1985) Ion solvation. Wiley, New York
59. Tissandier MD, Cowen KA, Feng WY, Gundlach E, Cohen MH, Earhart AD, Coe JV (1998) J Phys Chem A 102:7787–7794
60. Zhan CG, Dixon DA (2001) J Phys Chem A 105:11534–11540
61. Asthagiri D, Pratt LR, Ashbaugh HS (2003) J Chem Phys 119:2702–2708
62. Grossfield A, Ren P, Ponder JW (2003) J Am Chem Soc 125:15671–15682
63. Kelly CP, Cramer CJ, Truhlar DG (2006) J Phys Chem B 110:16066–16081
64. Donald WA, Leib RD, Demireva M, O'Brien JT, Prell JS, Williams ER (2009) J Am Chem Soc 131:13328–13337
65. Camaioni DM, Schwerdtfeger CA (2005) J Phys Chem A 109:10795–10797
66. Yamdagni R, Payzant JD, Kebarle P (1973) Can J Chem 51:2507–2511
67. Davidson WR, Kebarle P (1976) J Am Chem Soc 98:6125–6133
68. Valina AB (2001) J Phys Chem A 105:11057–11068
69. Guo BC, Conklin BJ, Castleman AW Jr (1989) J Am Chem Soc 111:6506–6510
70. More MB, Glendening ED, Ray D, Feller D, Armentrout PB (1996) J Phys Chem 100:1605–1614
71. Benitez D, Tkachouk E, Goddard WA III (2008) Chem Commun 6194–6196
72. Benitez D, Tkachouk E, Goddard WA III (2009) Organometallics 28:2643–2645
73. Bryantsev VS, Diallo MS, van Duin ACT, Goddard WA III (2009) J Chem Theory Comput 5:1016–1026
74. Zhao Y, Truhlar DG (2007) Org Lett 9:1967–1970
75. Tannor DJ, Marten B, Murphy R, Friesner RA, Sitkoff D, Nicholls A, Ringnalda M, Goddard WA III, Honig B (1994) J Am Chem Soc 116:11875–11882
76. Nakamura T (1975) Bull Chem Soc Jpn 48:1447–1451
77. Bryantsev VS, Diallo MS, Goddard WA III (2009) J Phys Chem A 113:9559–9567
78. Pasgreta E, Puchta R, Zahl A, van Eldik R (2007) Eur J Inorg Chem 1815–1822
79. Nigam S, Majumder C (2008) J Chem Phys 128:214307-1–214307-8
80. Marx D, Chandra A, Tuckerman ME (2010) Chem Rev 110:2174–2216